Computational Design of a Kit of Parts for Bending-Active Structures

QUENTIN BECKER*, EPFL, Switzerland
UDAY KUSUPATI*, EPFL, Switzerland
SEIICHI SUZUKI, EPFL, Switzerland
MARK PAULY, EPFL, Switzerland

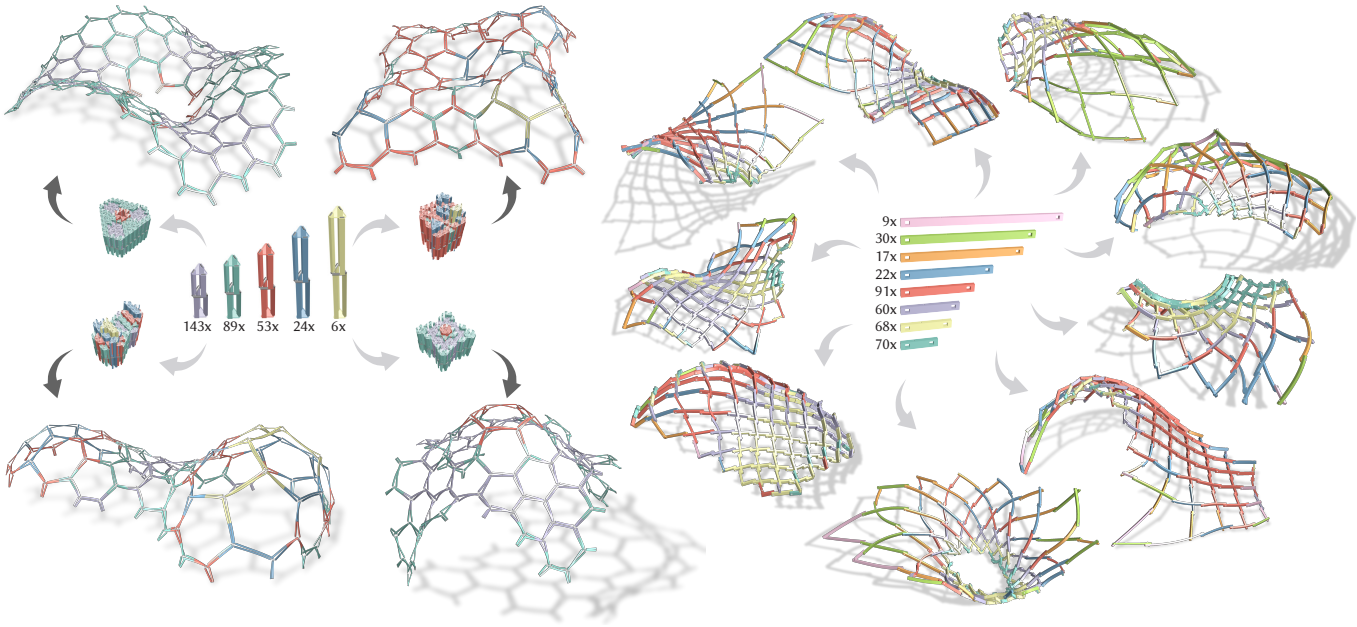

Fig. 1. A kit of parts allows cost-effective fabrication of bending-active assemblies. Our general optimization method finds the part geometries to best reproduce a given set of input designs and can be specialized to different material systems. Left: Umbrella meshes deploy from a compact assembly state towards a target equilibrium. Right: Bending-active orthogonal gridshells assembled from straight beams that deform to best approximate the target surface.

Bending-active structures are composed of elastic elements that deform to achieve a desired target shape. To support effective design, inverse algorithms have been proposed that optimize the geometry of each element specifically for each design. This makes it difficult to reuse elements across designs or gain efficiency in fabrication through mass production.

We address this issue and propose a computational framework to rationalize bending-active structures into a sparse kit of parts. Our method solves for the optimal part geometry such that multiple input designs can be faithfully realized with the same kit of parts. Assigning parts to different assemblies leads to a combinatorial explosion that makes exhaustive search intractable. Instead, we propose a relaxed continuous optimization incorporating a physics-based simulation in its inner loop to model the elastic deformation of the bending-active structure accurately. Our algorithm allows analyzing different design trade-offs of a kit of parts to tune the balance between fabrication complexity and fidelity to the original designs. We demonstrate our method on three different classes of bending-active structures, showcasing the effectiveness of our approach for part reuse and sustainable practices in fabrication-driven design.

CCS Concepts: • **Applied computing** → **Computer-aided design**; • **Computing methodologies** → *Modeling and simulation*; • **Mathematics of computing** → *Mixed discrete-continuous optimization.*

Additional Key Words and Phrases: kit of parts, bending-active structures, numerical optimization, physics-based simulation, fabrication-aware design

ACM Reference Format:
Quentin Becker, Uday Kusupati, Seiichi Suzuki, and Mark Pauly. 2024. Computational Design of a Kit of Parts for Bending-Active Structures. *ACM Trans. Graph.* 43, 6, Article 230 (December 2024), 16 pages. https://doi.org/10.1145/3687966

*joint first authors.

Authors' addresses: Quentin Becker, EPFL, Lausanne, Switzerland, quentin.becker@epfl.ch; Uday Kusupati, EPFL, Lausanne, Switzerland, uday.kusupati@epfl.ch; Seiichi Suzuki, EPFL, Lausanne, Switzerland, seiichi.suzuki@epfl.ch; Mark Pauly, EPFL, Lausanne, Switzerland, mark.pauly@epfl.ch.

0730-0301/2024/12-ART230 $15.00
https://doi.org/10.1145/3687966

1 INTRODUCTION

Bending-active structures are physical systems characterized by distinctive curved geometries, which arise from the elastic deformation of initially straight or planar elements. This formation approach not only enables the creation of static structures but also facilitates the construction of kinetic and deployable systems by leveraging the reversibility of elastic deformations [Lienhard 2014]. While the constituent elements must be thin and slender to allow significant deformation, the structures must counterbalance this material reduction to withstand loads by employing alternative stress-stiffening effects achieved through appropriate geometric design [La Magna 2017].

The equilibrium form of these structures emerges when all internal forces induced by elastic deformation of the elements and external forces, such as gravity, are in global balance. The presence of large deformations, along with the sensitivity of the structural form to even minor changes in the geometry and material properties of its constituents, makes the design process highly challenging. In response to this, physics-based simulations have been integrated into the research of bending-active structures to accurately predict equilibrium states [Lienhard et al. 2013; Manolas et al. 2022]. To match a simulated form with a desired input freeform geometry, inverse design algorithms have been proposed that directly solve for the design parameters of the bending-active structure [Becker et al. 2023; Panetta et al. 2019; Pillwein and Musialski 2021; Ren et al. 2022]. These parameters typically define the undeformed rest state of the constituent elements, which can be fabricated in a flat state and then assembled into the final structure.

One key advantage of bending-active structures is that their constituent elements are designed to maintain strain within the elastic limits of the material, allowing for reversible elastic deformation. This means that a structure can be undeployed and individual components could in principle be re-used in a different design. However, current inverse design methods compute optimized component geometries that are specific to one particular design only. This limits the re-use potential of parts and requires custom fabrication of each individual element, which can be slow and expensive compared to mass production techniques. Our work addresses these drawbacks and investigates the question of how to design a kit of parts that can be manufactured at scale and be re-used across multiple designs of bending-active structures.

This problem has been extensively studied for static structures composed of rigid components, in particular in the context of architectural research [Alegria Mira et al. 2016; Brütting et al. 2021]. Freeform designs are rendered feasible for fabrication by *rationalizing* them to groups of identical components. Such an optimized kit of parts can be used to assemble complex structures with an efficient fabrication pipeline, providing a cheaper and more sustainable alternative to custom fabrication. We study this problem for bending-active structures, where parts can deform into many different configurations in different assemblies. This additional complexity requires a fundamentally different approach.

Contributions. Our main contribution is a computational framework for optimizing a kit of parts for bending-active structures. We propose a numerical method that relaxes the discrete combinatorial nature of the part-to-element assignment problem into a continuous optimization problem. This fully differentiable optimization can be seamlessly combined with a physics-based simulation that tracks the equilibrium states of all input design instances mapped onto the kit of parts. Our formulation is general in that it can be applied to different classes of bending-active structures. We show how to customize the algorithm for three concrete examples of bending-active structures, highlighting the versatility of our approach. The full source code and experiments can be found at https://go.epfl.ch/kop.

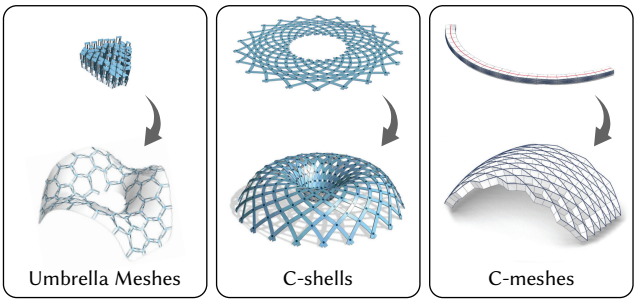

Fig. 2. Examples of bending-active structures using elastic beams: Umbrella Meshes [Ren et al. 2022], C-shells [Becker et al. 2023], and orthogonal grids (a superset of C-meshes [Liu et al. 2023b]) that can be actuated into a 3D target surface.

2 RELATED WORK

We discuss prior work on bending-active and deployable structures in the context of component reuse and rationalization. Works proposing component reuse in architecture are followed by a review of reconfigurable systems with reusable components as their building blocks. We mention computational methods for rationalization in the context of computer graphics and further narrow our focus on modular systems involving a kit-of-parts approach to conclude the section.

Deployable Structures. Deployable structures transform from a compact *rest* state that is typically easy to assemble, transport, and store to a *deployed* target state. While deployment mechanisms span across different scales and material systems [Yang et al. 2023], we focus on structures composed of elastic beams coupled via specific joining mechanisms. Trusses, space frames, and gridshells [Dyvik et al. 2021] are notable examples of such structures on an architectural scale. Several works deal with finding deployable variants of gridshells [Becker et al. 2024; Panetta et al. 2019; Pillwein and Musialski 2021; Schling et al. 2022; Tellier 2022] and the actuation sequence for their erection. The inverse-design problem of computing the rest state that deploys to a desired deployed state is of particular interest. Approaches involving geometric abstractions and numerical optimization have been proposed to solve the problem for different deployable structures [Baek et al. 2018; Becker et al. 2023; Liu et al. 2023b; Ren et al. 2022].

Figure 2 shows examples of bending-active deployable structures. While digital fabrication techniques have enabled the creation of bespoke solutions tailored to specific deployment states, our focus

shifts to optimizing kit of parts that can be reused across multiple designs and deployments. This shift to generalized kits introduces significant challenges. Specifically, the inherent difficulty of rationalizing a material system is further intensified by the large deformations characteristic of bending-active structures. In these cases, the complexity is twofold: ensuring that the structure's deployability is preserved throughout the rationalization process, and accurately maintaining and tracking the equilibrium states of the system.

Orthogonal Gridshells. Orthogonal gridshells define another subclass of bending-active structures that is of particular interest. Here, the beam profiles are oriented normal to the design surface, allowing beams to deform along their weak axis to approximate the surface geometry, while load transfer occurs locally via their strong axis [Schling 2018]. Networks of asymptotic curves to create asymptotic gridshells [Schling and Barthel 2020; Schling et al. 2022] and pseudo-geodesic gridshells [Mesnil et al. 2023] are examples of such structures using straight strips. Circular strips have also been used on surfaces of constant mean curvature [Schling et al. 2018], or for deployable orthogonal structures (along with straight ones) through the concept of C-meshes [Liu et al. 2023b]. We consider a generalization of these structures with curved planar lamellas.

Re-usable Structures. Our focus on a kit-of-parts approach addresses the challenge of promoting the reusability of structural components. Reuse-driven design [Fivet and Brütting 2020; Huang et al. 2021] is crucial for promoting component reuse both upstream (by procuring components for future use) and downstream (by designing with future reuse in mind). An interesting approach of re-usability are modular structures made of identical universal components that can be reconfigured for various design realizations. Alegria and co-workers [2016] introduce a universal scissor component that can be reconfigured to all basic scissor cells. Liu et al. [2022] use reconfigurable units with three multi-stable states (long, short, and bent) to design 3D space metawires for reconfigurable antennas. Kusupati and colleagues [2023] use identical, shape-agnostic, and reconfigurable umbrella cells to realize structures that deploy into a large range of desired geometries. Although universal reconfigurable components can be manufactured at scale and reused across various designs, they often involve significant complexity in terms of part geometry and fabrication. In contrast, our work adopts the principle that a simpler, less reconfigurable kit of parts can be mass-produced more cost-effectively, striking a balance between part reuse and fabrication complexity.

Computational Rationalization. An important aspect of our work involves the rationalization of target geometries into a finite set of parts. Research in computer graphics and computational geometry is relevant for the panelization of free-form surfaces [Liu et al. 2021; Singh and Schaefer 2010; Zhu et al. 2023] with applications in architecture [Eigensatz et al. 2010; Zimmer et al. 2012]. Fu and colleagues [2010] generate a set of K quads whose instances can produce a tiled quad surface that approximates the input surface. Freeform honeycomb structures [Jiang et al. 2014] provide a torsion-free support structure with identical nodes. Jiang et al. [2021] use panels that are manufacturable by precise isometric bending of surfaces made from a few molds of constant Gaussian curvature. Various works such as [Luo et al. 2015; Testuz et al. 2013; Zhang and Balkcom 2016] also explore volumetric rationalization of 3D shapes using shape filling blocks.

Other works focus on clustering the set of parts based on different metrics. Basso and colleagues [2009] perform an optimization on free-form gridshells to cluster elements into a predefined number of different length groups. Liu et al. [2023a] present a clustering–optimization framework to reduce the number of different nodes in space frame structures. Zimmer and co-workers [2014] rationalize free-form shapes to a single kit of parts using the *Zometool* set composed of linear elements of nine different lengths connected by one universal joint with different connection directions. Lu and Xie [2023] reduce the number of different members in a truss layout by considering shared lengths between members as well as shared cross-sections. Schling and Barthel [2020] provide a holistic theory of *repetitive structures* considering both the geometric and constructive parameters through computational design. Their systematic study aims to identify principle relationships of form and structure and develop new design strategies.

Kit-of-Parts Approach. It is not a new idea to use a kit of parts pre-designed and engineered to be mass-produced for construction. Howe et al. [1999] draw parallels to an object-oriented programming environment with well-defined interfaces to be followed (e.g. load transfer rules, cost constraints, boundary constraints). Brütting and colleagues [2021] present a new computational workflow to design a bespoke kit of parts that can be employed to build structures of diverse typologies using optimization of structural members and joints i.e., the kit of parts that fit multiple geometric and structural requirements. St-Hilaire and Nejur [2022] propose form-matching of a temporary architectural structure with a kit of parts coupling wood with simple bendable steel strips. Gaudreault and Nejur [2023] introduce a constructive system aimed at maximizing the integration of reclaimed materials for the construction of triangular reticular structures. While these works take a kit-of-parts design approach, they do not handle free-form bending-active structures. We provide a general framework for rationalizing bending-active structures employing physics-based simulation for form-finding in the inner loop of the optimization.

3 OVERVIEW

Bending-active structures based on elastically deforming beams share many commonalities, even when their deployment mechanism are fundamentally different. This observation motivates our formulation of a general kit-of-parts optimization approach that can be customized towards of specific classes of bending-active structures.

Our algorithm takes as input a set of existing design instances, given by the individual geometries of all elastic elements in their rest state, and corresponding assembly graphs that define the connectivity of elements in each final structure. The goal is then to optimize for a sparse kit of parts, that is, to find the optimal geometry of each part as well as an assignment function that determines which element in each input design will be realized by which part.

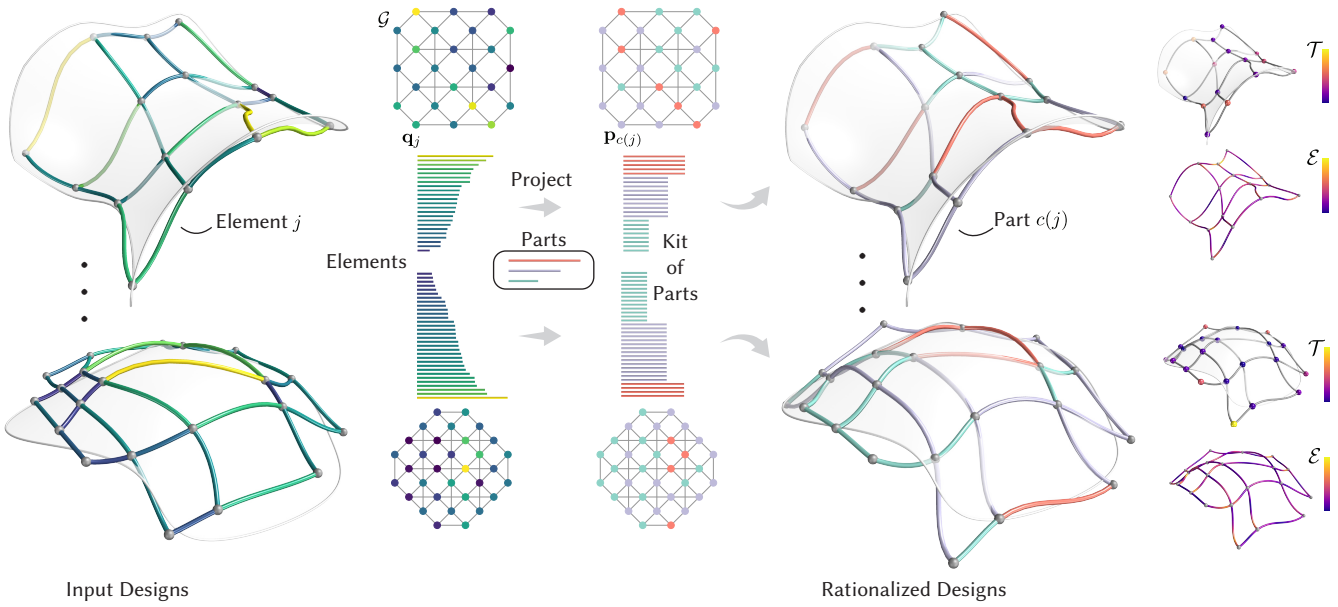

Fig. 3. Rationalization of a bending-active structure using a kit of parts: The graph $\mathcal{G}$ defines the assembly connectivity of the design with nodes representing constituent elements/beams. Projecting these designs onto a kit of parts replaces each element j with parameters $\mathbf{q}_j$ by a part $c(j)$ from the part set with parameters $\mathbf{p}_{c(j)}$. Here $\mathbf{c}$ represents the assignment function from elements to parts. The part set and the subsequent kit of parts are computed through an optimization that minimizes an objective comprising target fitting $\mathcal{T}$ and elastic energy $\mathcal{E}$ of the equilibrium state.

Such a kit of parts will be effective, if the number of parts is significantly smaller than the number of elements, while at the same time enabling faithful reproduction of the input designs.

We first define a template optimization problem in Section 4. Our formulation abstracts from class-specific implementation details and focuses on the core objectives that are common across different classes of bending-active structures. Specifically, we show in Section 5 how the combinatorial problem of assigning parts to elements can be solved with a continuous relaxation that allows integrating a physics-based simulation to track equilibrium states of the given input designs. We then illustrate in Section 6 how this template optimization can be overloaded with specific objectives for three concrete bending-active structures: (i) umbrella meshes, (ii) orthogonal grids, and (iii) C-shells. Implementation aspects of the numerical optimization are discussed in Section 7 with more details provided in the supplemental material.

We show in Section 8 how our algorithm enables users to analyze different design choices for the optimization of a kit of parts. This helps to find the most appropriate trade-off between the complexity of the kit of parts and the deviation to the input designs.

4 PROBLEM STATEMENT

In this section we introduce terminology and formulate the general problem of optimizing a kit of parts for bending-active structures.

We assume as input a set $S_1, S_2, \ldots$ of bending-active structures that represent the variability in designs that should be realizable by the kit of parts. Each structure S_k is represented by a graph $\mathcal{G}$ whose nodes denote the elastic elements of the structure that are joined according to the connectivity defined by the graph edges. Each node has attributes $\mathbf{q}_j \in \mathbb{R}^d$, a set of continuous parameters that define the element geometry. For example, $\mathbf{q}_j$ could denote the length and width of a straight beam and the location of rotational joints along the beam. For ease of notation, we accumulate all element parameters in a vector $\mathbf{q} = (\mathbf{q}_1, \ldots, \mathbf{q}_n)$ where n is the total number of elements across all input designs.

4.1 Equilibrium Computation

To simulate the equilibrium of a structure S_k, we convert the corresponding element parameters into a discrete representation suitable for simulation. In our case, we model elastic beams using the discrete elastic rod model introduced by Bergou and colleagues [2010; 2008]. Each beam is sampled with a polyline. The rest variables of the structure are then the lengths and angles of these polylines that we collect in a vector $\mathbf{r}$. The simulation variables representing a deformed state of the design, i.e., the nodal positions and local frames of all discrete elastic rods, are collected in a vector $\mathbf{x}$. The elastic energy of the deformation is defined as $\mathcal{E}(\mathbf{x}, \mathbf{r})$ and combines stretching, bending, and twisting terms as proposed in [Bergou et al. 2010].

The deformed state of S_k at equilibrium is the solution $\mathbf{x}^*$ of a constrained minimization problem. The optimization objective combines the elastic deformation energy $\mathcal{E}(\mathbf{x}, \mathbf{r})$ with external deployment forces modeled by an energy term $\mathcal{D}(\mathbf{x})$. We also integrate Dirichlet constraints to fix a certain subset of the deformed state variables $\mathbf{x}_f \subset \mathbf{x}$ to user-specified target values $\mathbf{x}_f^{\text{tgt}}$, allowing pinning vertices to fixed positions or simulating deployment. We aggregate the rest variables with the fixed variables in a vector of design variables $\mathbf{d}$. The equilibrium state $\mathbf{x}^*$ is defined as a function

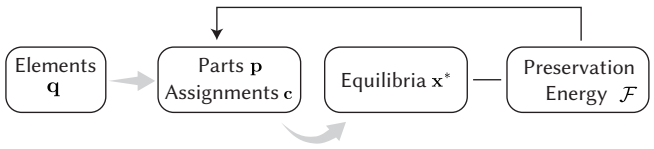

Fig. 4. Optimization flow for the original kit of parts problem. The objective is to find the optimal part parameters $\mathbf{p}$ and assignments $\mathbf{c}$ that minimize the design preservation energy $\mathcal{F}$ across all designs.

of design variables $\mathbf{d}$ as

$$\mathbf{x}^*(\mathbf{d}) := \underset{\mathbf{x}}{\operatorname{argmin}}\, \mathcal{E}(\mathbf{x}, \mathbf{r}) + \mathcal{D}(\mathbf{x}) \quad \text{s.t.} \quad \mathbf{x}_f = \mathbf{x}_f^{\text{tgt}}. \tag{1}$$

4.2 Kit of Parts Objective

A kit of parts is an ensemble of m parts $\mathbf{p} := (\mathbf{p}_1, \ldots, \mathbf{p}_m)$, where $\mathbf{p}_i \in \mathbb{R}^d$ define the parts' geometry analogous, but potentially different to the parameterization used for elements of the input designs.

To realize the structures S_k with the kit of parts $\mathbf{p}$, we define an assignment function $c : [1, n] \to [1, m]$ that indicates which part of $\mathbf{p}$ is assigned to which element in $\mathbf{q}$. These assignments are aggregated over all structures in a vector $\mathbf{c} = (c(1), \ldots, c(n))$. The assignment process is described in more detail in Section 5.2. Figure 3 illustrates $\mathbf{q}$, $\mathbf{p}$, and $\mathbf{c}$ for a simple bending-active system. See also Figure 6 and Section 6 for the specific classes we consider below.

The optimization aims to compute the part parameters of $\mathbf{p}$ with $m \ll n$ and the corresponding assignment $\mathbf{c}$ such that element $\mathbf{q}_j$ can be rationalized as an instance of part $\mathbf{p}_{c(j)}$. This projection onto the kit of parts inevitably incurs a deviation in the resulting equilibrium shapes from the input designs. Our goal is to reduce this discrepancy to a minimum while retaining a low elastic energy of the system. We thus formulate a design preservation energy as a function of $(\mathbf{x}, \mathbf{r})$ as,

$$\mathcal{F}(\mathbf{x}, \mathbf{r}) = \mathcal{T}(\mathbf{x}) + \mathcal{E}(\mathbf{x}, \mathbf{r}), \tag{2}$$

where $\mathcal{T}$ is a target fitting term measuring the distance of the deformed state $\mathbf{x}$ to a given target surface, and $\mathcal{E}$ is the elastic energy of $\mathbf{x}$. In the supplemental material we describe how to apply suitable weight factors for these terms to make $\mathcal{F}$ scale-invariant. We discuss how $\mathcal{F}$ can be adapted to different systems in Section 6.

Once a design S_k is rationalized using the kit of parts $\mathbf{p}$, its rest variables $\mathbf{r}_k$ and design variables $\mathbf{d}_k$ are a function of the part parameters $\mathbf{p}$ and the assignment $\mathbf{c}$. As a consequence, the equilibrium state $\mathbf{x}_k^*(\mathbf{d}_k)$ is a function of $(\mathbf{p}, \mathbf{c})$ as well. We therefore formulate the objective function for the kit of parts optimization as the sum of the design preservation energies across all designs:

$$\mathcal{J}(\mathbf{p}, \mathbf{c}) = \sum_k \mathcal{F}\left(\mathbf{x}_k^*(\mathbf{p}, \mathbf{c}), \mathbf{r}_k(\mathbf{p}, \mathbf{c})\right). \tag{3}$$

Figure 4 illustrates the optimization problem. Optionally, weights can be assigned to indicate the relative importance of each design and re-formulate the objective as a weighted sum of design preservation energies.

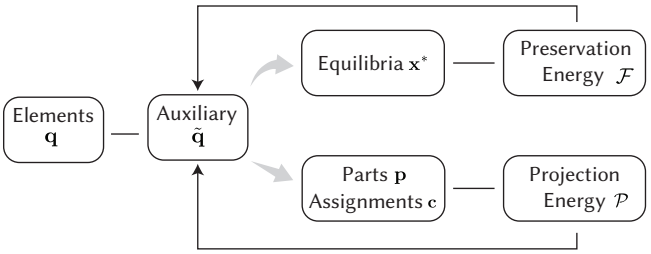

Fig. 5. Optimization flow for the relaxed problem. The relaxation enables a fully differentiable optimization that can be seamlessly combined with a physics-based simulation. The elements $\mathbf{q}$ and parts $\mathbf{p}$ are illustrated in Figure 6. Figure 7 visualizes the part assignments $\mathbf{c}$ and equilibria $\mathbf{x}^*$ along with the energies $\mathcal{F}$ and $\mathcal{P}$.

5 KIT OF PARTS OPTIMIZATION

The equilibrium state $\mathbf{x}^*$ in Equation (3) is sensitive to changes in the kit-of-parts variables $(\mathbf{p}, \mathbf{c})$. A change in the assignment function can lead to a large jump in the equilibrium state $\mathbf{x}^*$ and subsequently the design preservation energy $\mathcal{J}$. In addition, the space of assignments $\mathbf{c}$ grows exponentially with n, making an exhaustive search over the m^n possibilities intractable. The projection of elements $\mathbf{q}$ onto parts $\mathbf{p}$ in the context of bending-active structures is challenging and can result in buckled equilibrium states. We discuss more about buckling issues in Section 8 and illustrate in Figure 11 how our approach mitigates them.

5.1 Projection-Relaxed Problem

We address the forementioned challenges by formulating a relaxation of the problem of minimizing Equation (3) to a tractable continuous optimization. This relaxation is achieved by tracking auxiliary continuous variables $\tilde{\mathbf{q}}$ of the elements in the simulation.

We define the kit-of-parts parameters $(\mathbf{p}, \mathbf{c})$ as dependent variables of $\tilde{\mathbf{q}}$ and introduce a projection energy $\mathcal{P}$ to bind the auxiliary variables $\tilde{\mathbf{q}}$ to the parts and assignment variables $(\mathbf{p}, \mathbf{c})$. The rest variables $\mathbf{r}_k$ and the equilibrium state $\mathbf{x}_k^*(\mathbf{r}_k)$ of design S_k are defined as functions of $\tilde{\mathbf{q}}$. The new objective is then written as a function of $\tilde{\mathbf{q}}$:

$$\mathcal{J}(\tilde{\mathbf{q}}) = \sum_k \mathcal{F}\left(\mathbf{x}_k^*(\tilde{\mathbf{q}}), \mathbf{r}_k(\tilde{\mathbf{q}})\right) + \mathcal{P}(\tilde{\mathbf{q}}). \tag{4}$$

As opposed to the former objective of Equation 3, part parameters $\mathbf{p}$ and part assignments $\mathbf{c}$ are dependent variables of $\tilde{\mathbf{q}}$ and are updated in the optimization loop. The relaxed formulation defines the equilibrium simulation as a function of the continuous variables $\tilde{\mathbf{q}}$ and makes $\mathcal{J}$ robust to large jumps due to changes in the assignment function. The optimization flow is illustrated in Figure 5. The various terms in $\mathcal{J}(\tilde{\mathbf{q}})$ specific to our bending-active systems are defined in Section 6 and illustrated in Figure 7 on a single design instance for each system.

5.2 Projection Energy

To define $\mathcal{P}$, we first introduce a non-dimensionalized part-element projection energy $\rho : \mathbb{R}^d \times \mathbb{R}^d \to \mathbb{R}_+$. A low value of $\rho(\mathbf{p}_i, \tilde{\mathbf{q}}_j)$ indicates higher similarity between an element j and a part i. For independent parts $\mathbf{p}$, assignment $\mathbf{c}$, and elements $\tilde{\mathbf{q}}$, the projection

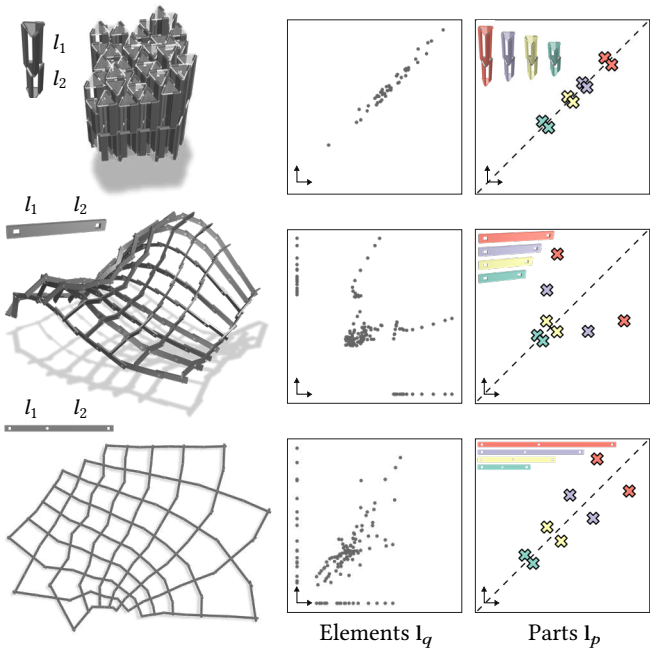

Fig. 6. Elements, parts, and assembly states of the three classes of bending active structures we consider. From top to bottom: Umbrella Meshes, orthogonal grids, C-shells. The plots on the right illustrate the distribution of parameters in the input models compared to an optimized kit of parts, where element symmetries can be exploited to further reduce the number of parts.

energy $\tilde{\mathcal{P}}(\mathbf{p}, \mathbf{c}, \tilde{\mathbf{q}})$ is aggregated over all elements as,

$$\tilde{\mathcal{P}}(\mathbf{p}, \mathbf{c}, \tilde{\mathbf{q}}) := \frac{w_c}{n} \sum_{j=1}^{n} \rho(\mathbf{p}_{c(j)}, \tilde{\mathbf{q}}_j), \tag{5}$$

where the weight w_c controls the relative importance given to the projection energy term during optimization. Minimizing $\tilde{\mathcal{P}}$ ensures that the elements are well represented by the parts they have been assigned.

The projection energy $\mathcal{P}(\tilde{\mathbf{q}})$ from Equation (4) is then obtained as a minimum over all possible parts and assignments for a given set of elements $\tilde{\mathbf{q}}$,

$$\mathcal{P}(\tilde{\mathbf{q}}) := \min_{\mathbf{p},\mathbf{c}} \tilde{\mathcal{P}}(\mathbf{p}, \mathbf{c}, \tilde{\mathbf{q}}). \tag{6}$$

We minimize $\tilde{\mathcal{P}}$ in an alternating fashion over assignment and part updates.

Updates. The assignment $\mathbf{c}$, or the function c, is updated by keeping $\mathbf{p}$ fixed and solving for the optimal assignment,

$$c(j) := \operatorname*{argmin}_i \rho(\mathbf{p}_i, \tilde{\mathbf{q}}_j). \tag{7}$$

The parts $\mathbf{p}$ are then updated by keeping $\mathbf{c}$ fixed and solving for the optimal parts,

$$\mathbf{p}_i(\tilde{\mathbf{q}}) := \operatorname*{argmin}_{\mathbf{y} \in \mathbb{R}^d} \sum_{j \in c^{-1}(\{i\})} \rho(\mathbf{y}, \tilde{\mathbf{q}}_j), \tag{8}$$

where $c^{-1}(\{i\})$ is the set of elements currently assigned to part i. In all of our examples, the update step in Equation (8) can be solved analytically and efficiently differentiated through. The alternating updates are repeated until convergence for every evaluation of $\mathcal{P}(\tilde{\mathbf{q}})$. Note that when ρ is the squared L^2 distance, the update rules are equivalent to the k-means clustering algorithm [MacQueen et al. 1967].

Initialization. The alternating update scheme to compute $\mathcal{P}(\tilde{\mathbf{q}})$ requires an initial guess for $(\mathbf{p}, \mathbf{c})$. Our initialization is inspired by the k-means++ algorithm [Arthur et al. 2007], so that parts are as spread out over the set of elements as possible. A first element is chosen uniformly at random and assigned to the first part $\mathbf{p}_1$. A new element $\tilde{\mathbf{q}}_j$ is chosen at random among the remaining elements according to a probability proportional to the squared distance $\min_i \rho(\mathbf{p}_i, \tilde{\mathbf{q}}_j)^2$, where i spans the initialized parts and j indexes the remaining unassigned elements. The chosen element j is then assigned to part i and i is added to the set of initialized parts. This process is repeated until m parts have been constructed. We observe in Figure 7 (left) that such a process allows the parts to span the element space well.

6 SPECIALIZATION TO BENDING-ACTIVE SYSTEMS

We specialize our general computational pipeline to optimize a kit of parts for the chosen bending-active systems: Umbrella Meshes [Ren et al. 2022], Orthogonal Grids, and C-shells [Becker et al. 2023]. Physics-based simulations of the involved bending-active structures are based on the methods presented in the respective papers which have been validated by fabricating prototypes.

We formulate the objective from Equation (3) specific to these three systems. In particular, we define the elements and parts parameterizations, the deployment process, and the element-to-part projection energy. The datasets of shapes for all systems are shown in the supplemental material.

6.1 Umbrella Meshes

Umbrella Meshes are composed of modular volumetric scissor linkages, coined *umbrella cells*. Each umbrella cell deploys from a compact vertical configuration to a flat expanded state whose footprint depends on the height of the cell. When umbrella cells of different heights are assembled together and deployed, metric frustration due to expansion incompatibilities causes the structure to deform into a doubly-curved bending-active surface structure. The top corner of Figure 6 illustrates the elements that make up an umbrella cell, which can be rationalized into a kit of parts for subsequent assembly and deployment. The plates, X-joints and T-joints are identical across all the designs.

Preservation Energy. Each umbrella cell is defined in its rest state by the lengths of the arms connected to the top plate (top heights) and the lengths of the arms connected to the bottom plate (bottom heights). [Ren et al. 2022] explain how different top and bottom heights lead to programming mean curvature in the deployed state. The rest variables $\mathbf{r}$ are defined as the aggregation of these lengths. The design variables $\mathbf{d}$ may also include pinned vertices at the boundary as for model 2 in Figure 11. The structure is deployed in a similar strategy to the one described in [Ren et al. 2022]: top and

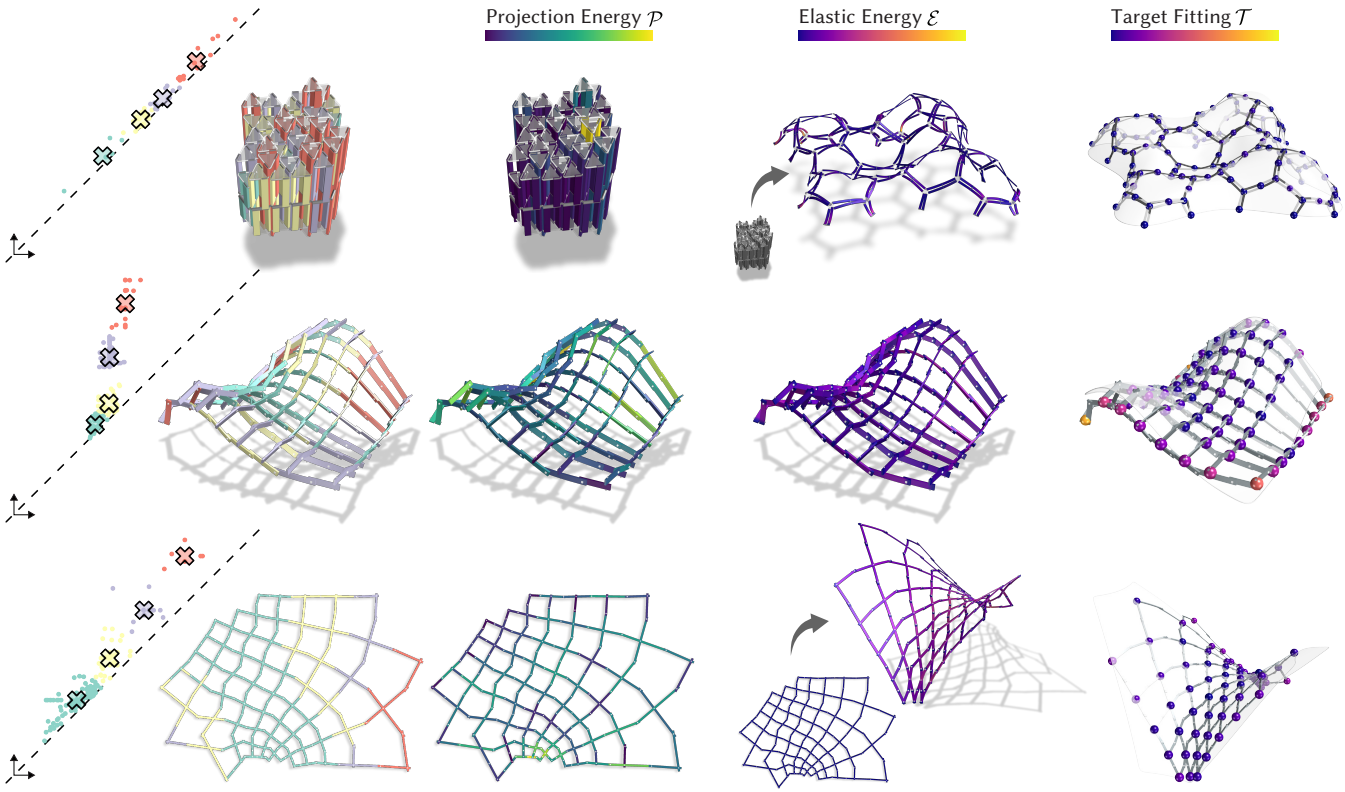

Fig. 7. Optimization objectives in the relaxed problem: For a given input design, the objective function $\mathcal{J}$ is composed of the design preservation energy $\mathcal{F}$ ($= \mathcal{T} + \mathcal{E}$) and the projection energy $\mathcal{P}$. The plots on the left show distributions of element parameters $\tilde{\mathbf{q}}$ and the optimal part assignments $(\mathbf{p}, \mathbf{c})$ minimizing the projection energy $\mathcal{P}$. The dots and crosses represent $\tilde{\mathbf{q}}$ and $\mathbf{p}$ as defined in Figure 6. The subsequent columns illustrate each of the terms in $\mathcal{J}$ for the three classes of bending-active structures.

bottom plates are brought together through a linear actuator and rigid motions are pinned using small surface attraction forces when there are no boundary constraints. These additional conservative forces responsible for deployment are modeled by the energy term $\mathcal{D}$ in Equation (1). The resulting deployed state $\mathbf{x}^*$ is then used to evaluate the objective $\mathcal{J}$ in Equation (4).

Projection Energy. Each umbrella unit/element, is parameterized by the length of the arms of the top plate and the bottom plate, $\mathbf{l}_q \in \mathbb{R}^2_+$. Naturally, we define parts as two lengths $\mathbf{l}_p \in \mathbb{R}^2_+$. Parts can be used as is or in a mirrored configuration, which is illustrated by the mirror symmetry about the bisector of the first quadrant in Figure 6 (top right). The projection energy between elements and parts is defined as the squared L^2 norm of the difference between the two lengths in both part configurations,

$$\rho(\mathbf{l}_p, \mathbf{l}_q) = \frac{1}{2l_\rho} \min\left(\left\|\mathbf{l}_p - \mathbf{l}_q\right\|_2^2, \left\|\text{flip}(\mathbf{l}_p) - \mathbf{l}_q\right\|_2^2\right), \tag{9}$$

where $\text{flip}(\mathbf{p}_i)$ flips the lengths of the part $\mathbf{p}_i$, and l_ρ is chosen as the median of the arm lengths across the input designs. In this case, the update rule in Equation (8) can be solved analytically by sorting the assigned elements' lengths and taking the mean. Note that the sorting indices need to be stored to ensure the correct assignment of the parts to the elements.

6.2 Orthogonal Grids

Orthogonal grids are bending-active structures composed of elastic lamellas attached at the crossings. The lamellas are oriented such that their strong axis is orthogonal to the input design surface. C-meshes [Liu et al. 2023b] shown in Figure 2 are a special case of orthogonal grids that further imposes the structure to be collapsible into a flat state. In general, orthogonal grids require curved elements to best approximate the underlying target surface. We rationalize the curved rods as piecewise straight beams rigidly connected at their *corners*. Exactly one corner is allowed between two neighboring joints along each rod, to spatially separate inner- and inter-rod connections.

Preservation Energy. The design state $\mathbf{d}$ of an orthogonal grid comprises rod segment rest lengths together forming the rest variables vector $\mathbf{r}$, and corner angles. Inter-rod connections are simulated using rotational joints, effectively constraining the intersection point of two rods while allowing rotation. Corners, or inner-rod connections, are simulated as rigid joints with the opening angle between

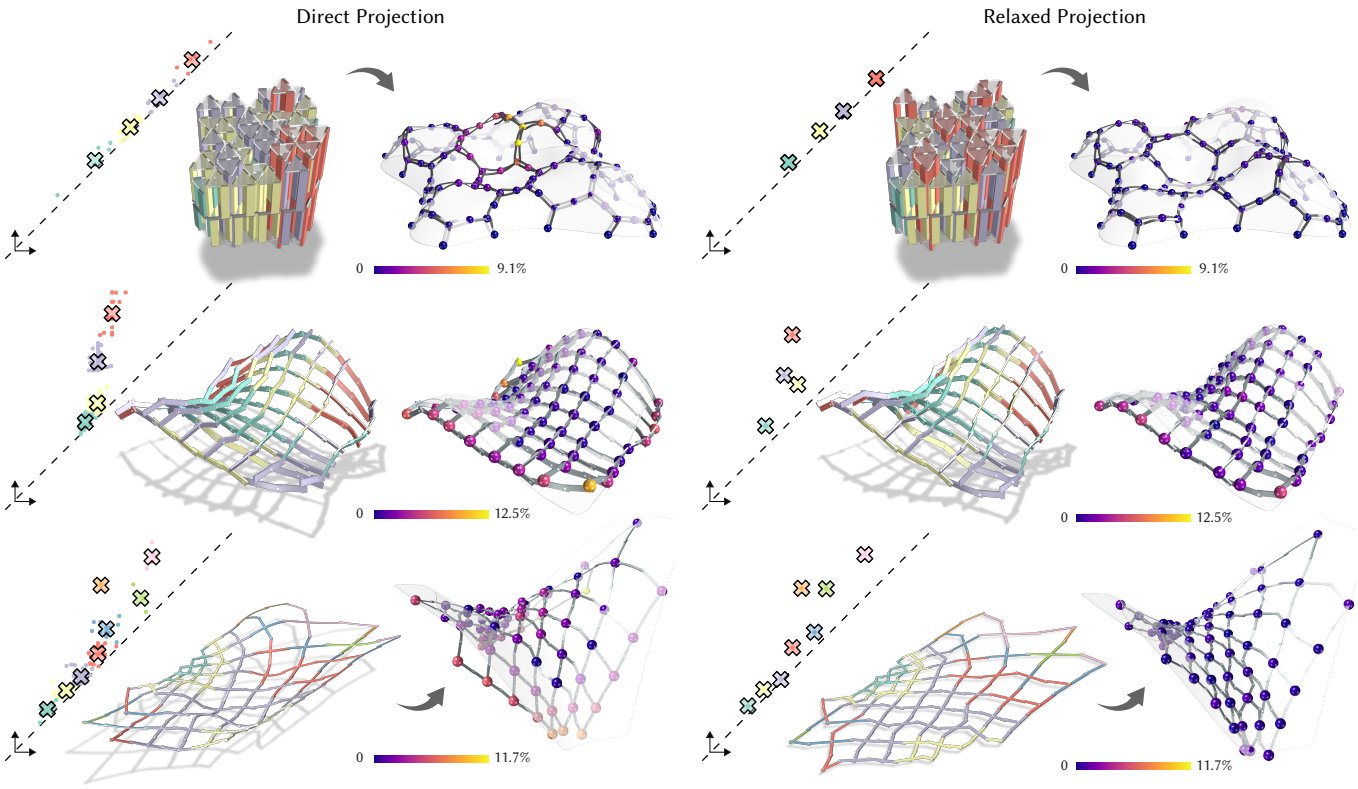

Fig. 8. The parts $\mathbf{p}(\mathbf{q})$ and assignments $\mathbf{c}(\mathbf{q})$ directly extracted from the original design yields poor preservation of the target shape (left). By re-arranging and collapsing elements around their assigned parts, our relaxed optimization process allows for a better preservation of the initial design (right).

two rod segments treated as a fixed variable. The corner angles form the set of fixed simulation variables $\mathbf{x}_f$ (Dirichlet constraints) of the equilibrium problem in Equation (1). We rule out rigid motions of the structures during simulation using the same strategy as in Umbrella Meshes.

Projection Energy. Each straight element is parameterized by the distance from the first corner joint to the rotational joint and the distance from the rotational joint to the second corner as shown in Figure 6 (left). The order of the corners is given by following the curves in the original design. Boundary elements are distinguished from inner elements as they have only one corner joint, and are defined by a single length.

We consequently define each part as two lengths $\mathbf{l}_p \in \mathbb{R}^2_+$. Similar to parts in Umbrella Meshes, parts can be used as is or mirrored. The projection energy is defined equivalently to the Umbrella Meshes case, and the parts update rule is solved similarly using the sort strategy. We use the median of the rod lengths across the input designs as the reference length l_ρ in Equation (9).

To ease the assembly process, corner angles are also grouped into their own discrete set of parts. Our kit of parts is then composed of two types of parts: straight beams (linear parts) and corner angles (angular parts). The corner angles are parameterized by the angle between the two straight beams they connect, as shown in Figure 9. Parts are defined subsequently by a single angle $\theta_p \in [0, \pi]$, and

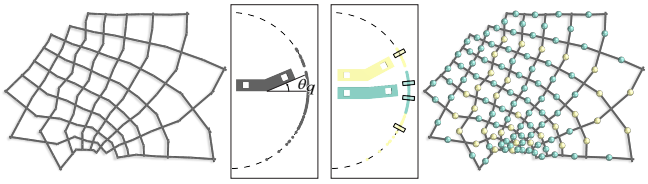

Fig. 9. Angular elements $\theta_q \in [-\pi, \pi]$ are computed at the corners of rationalized C-shells. The angular part is defined by a single angle $\theta_p \in [0, \pi]$ and can be flipped. We represent the angular elements, the 2 parts and their flipped configurations on the unit circle.

can be mirrored during assembly. Our projection energy is then defined as the squared difference between the two unsigned angles $\rho(\theta_p, \theta_q) = \frac{1}{2}\left(\theta_p - |\theta_q|\right)^2$. Based on that definition, the update rule in Equation (8) is the average of the assigned elements' unsigned angles.

6.3 C-shells

C-shells are deployable gridshells composed of curved elastic beams connected through rotational joints [Becker et al. 2023]. The assembly state is stress-free by definition and the structure is deployed via torque actuation, by constraining the average opening angle at the rotational joints. For a completely custom fabricated C-shell

tailored to deploy to a specific surface, the curved beams are laser cut precisely following some optimized splines. Similar to Orthogonal Grids, we rationalize each of the curved beams using piecewise straight beams joined at rigid corners. Rotational and corner joints now share the same axis in the rest state.

Preservation Energy. Each rationalized C-shell is defined by the lengths of the straight beams, the corner angles, and the average opening angle of the single-axis rotational joints in the deployed state. These design variables are aggregated in $\mathbf{d}$. Rigid connections at the corners are simulated using Dirichlet constraints in Equation (1). Depending on the values of beam lengths and corner angles, a rationalized C-shell no longer has a guaranteed zero-energy *rest equilibrium state* when assembled. We therefore compute this state $\mathbf{x}_\mathrm{r}^*$ by solving an equilibrium problem for the assembly configuration. The deployed equilibrium state $\mathbf{x}_\mathrm{d}^*$ is obtained by further constraining the average opening angle at the rotational joints as described in Becker et al. [2023]. In order to mitigate incompatibilities in the rest state $\mathbf{x}_\mathrm{r}^*$ and ease assembly, we incorporate the energy of the rest equilibrium state in the preservation energy as

$$\mathcal{F}\left(\mathbf{x}_\mathrm{r}, \mathbf{x}_\mathrm{d}, \mathbf{r}\right) = \mathcal{T}\left(\mathbf{x}_\mathrm{d}\right) + \mathcal{E}\left(\mathbf{x}_\mathrm{d}, \mathbf{r}\right) + \mathcal{E}\left(\mathbf{x}_\mathrm{r}, \mathbf{r}\right), \tag{10}$$

and we update $\mathcal{J}$ to track both equilibria as

$$\mathcal{J}(\tilde{\mathbf{q}}) = \sum_k \mathcal{F}\left(\mathbf{x}_{\mathrm{r},k}^*(\tilde{\mathbf{q}}), \mathbf{x}_{\mathrm{d},k}^*(\tilde{\mathbf{q}}), \mathbf{r}_k(\tilde{\mathbf{q}})\right) + \mathcal{P}(\tilde{\mathbf{q}}), \tag{11}$$

where k indexes the different designs in the input set.

Projection Energy. We define each linear part as two lengths $\mathbf{l}_p \in \mathbb{R}_+^2$, and each corner angle as a single angle $\theta_p \in [0, \pi]$. The projection energies between elements and parts of the same type, and the parts' update rules are defined identically to the Orthogonal Grids case.

7 TWO-STAGE OPTIMIZATION

We first show a direct rationalization approach in Figure 8 that computes parts $\mathbf{p}$ and assignments $\mathbf{c}$ directly from the input elements $\mathbf{q}$ by minimizing $\tilde{\mathcal{P}}(\mathbf{p}, \mathbf{c}, \mathbf{q})$. This approach does not take the design preservation energy $\mathcal{F}$ into account and can lead to undesired buckling in the output designs. Then, we illustrate the performance of the unrelaxed approach from Section 4 which optimizes the part parameters $\mathbf{p}$ using the assignments from minimizing $\tilde{\mathcal{P}}(\mathbf{p}, \mathbf{c}, \mathbf{q})$ directly. We then compare our relaxed approach in Figure 11. We propose a two-stage optimization approach that first optimizes the relaxed problem and then fine-tunes the parts $\mathbf{p}$ while keeping the assignments $\mathbf{c}$ fixed to minimize the total preservation energy $\mathcal{F}$. We show the results of our approach in Figure 12.

7.1 First Stage: Relaxation

The original design rationalization problem described in Section 4 is a combinatorial optimization problem, where the number of possible part-to-element assignments grows as m^n. This makes the problem intractable for large elements count n and a non-trivial kit of parts.

Instead, our relaxation allows leveraging tools from the continuous optimization literature to efficiently solve

$$\tilde{\mathbf{q}}^* := \underset{\tilde{\mathbf{q}}}{\operatorname{argmin}}\, \mathcal{J}(\tilde{\mathbf{q}}), \text{ s.t. } \mathbf{p}_\mathrm{min} \le \tilde{\mathbf{q}} \le \mathbf{p}_\mathrm{max}, \tag{12}$$

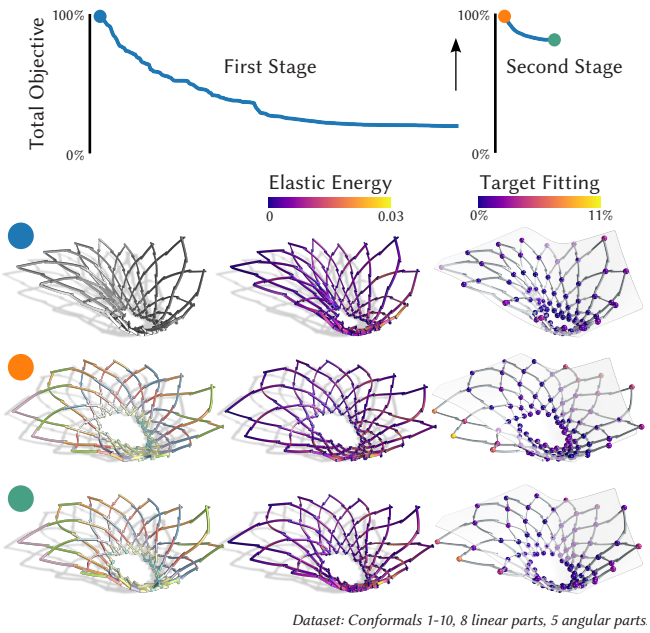

Fig. 10. Our two stage optimization fine-tunes designs after first optimizing the relaxed problem. The arrow indicates the projection of the solution of the first stage $\tilde{\mathbf{q}}^*$ onto the part set to obtain $\mathbf{p}(\tilde{\mathbf{q}}^*)$, the initial guess for the second stage. We plot the objective of each stage normalized with respect to the initial value for that stage. The rows show the designs at the start, between the two stages, and at the end of the full optimization process.

where $\tilde{\mathbf{q}}$ now contains all elements of different kinds (linear and angular if applicable), and $\mathbf{p}_\mathrm{min}$ and $\mathbf{p}_\mathrm{max}$ are lower and upper bounds. These are derived from the parts feasibility and fabricability constraints e.g., for the minimum distance between corners and joints for linear parts. We assume that elements of the same kind share the same constraints. In the supplemental material, we show that for all the part-element projection energies ρ we use in our experiments, the resulting parts obtained from the optimal elements $\mathbf{p}(\tilde{\mathbf{q}}^*)$ using the update rule in Equation (8) are *guaranteed* to satisfy the original feasibility constraints. This fact effectively positions our method as a co-rationalization approach providing an end-to-end parametric control over the output designs with respect to the part feasibility constraints.

Figure 11 shows how our projection onto a kit of parts after our first-stage relaxation preserves designs better compared to directly solving the original unrelaxed problem. This forms the base for the second stage of our optimization.

7.2 Second Stage: Fixed Assignment Fine-Tuning

The first stage optimization strives to concentrate all the *auxiliary elements* tightly around the *parts* in order to mitigate the discontinuous elements-to-parts conversion. However, the output goal is still a part set, and thus the auxiliary variables need to be converted to the assigned parts. To this end, we perform a second stage of fine-tuning, where we fix the assignment $\mathbf{c}(\tilde{\mathbf{q}}^*)$ and optimize the

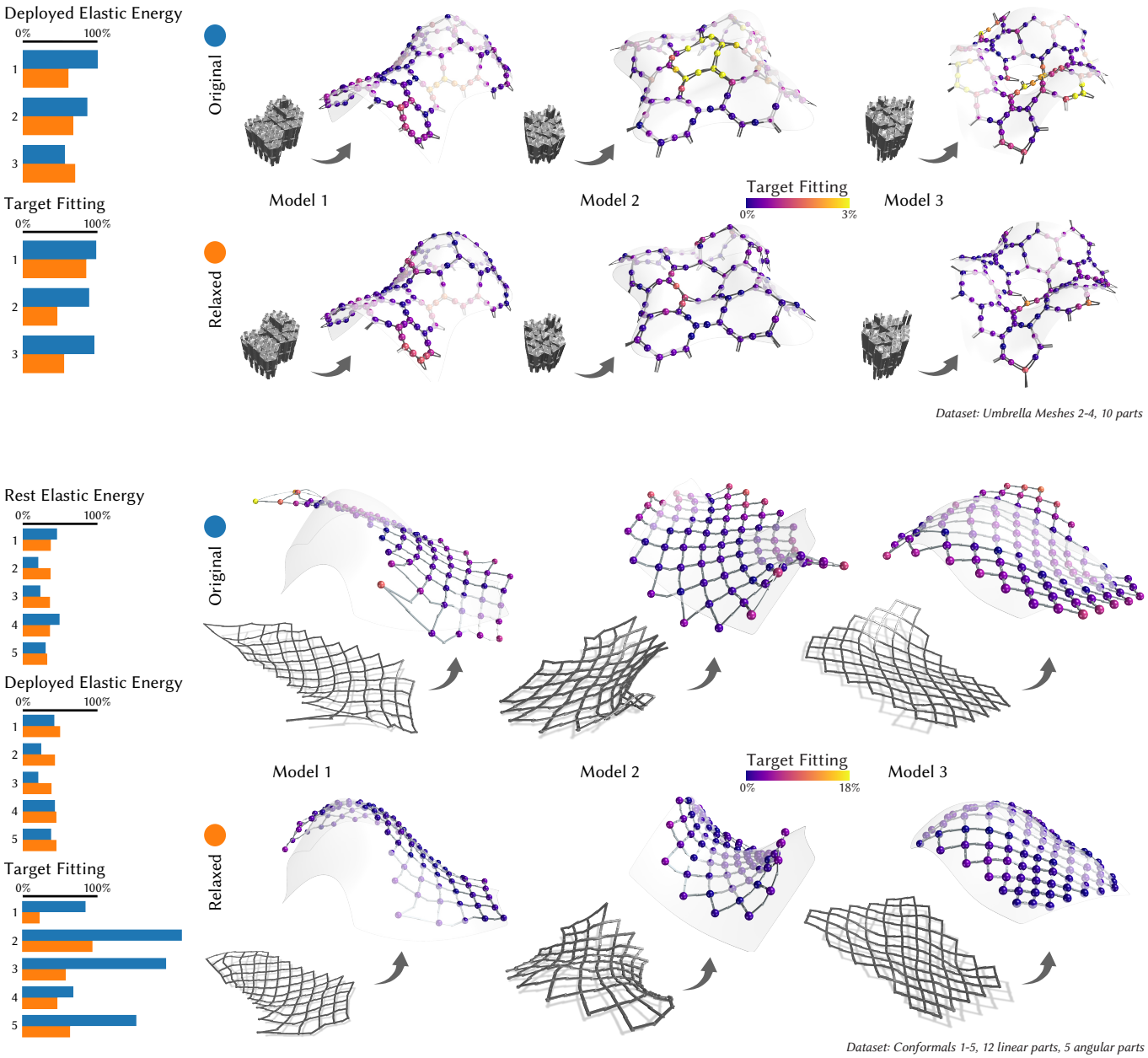

Fig. 11. Solving for the original minimization problem over the parts $\mathbf{p}$ in Equation (3) using the original assignments $\mathbf{c}(\mathbf{q})$ produces undesired buckling. Our relaxation allows smoothly bringing designs together towards a shared kit of parts. We show designs after the first stage optimization involving the relaxation and project the elements on to the parts at the end of it. We report target fitting as a percentage of each model's bounding box diagonal. The optimization quantities are normalized using the respective initial values for each "projected" design.

part parameters starting from $\mathbf{p}(\tilde{\mathbf{q}}^*)$, as

$$\mathbf{p}^* := \underset{\tilde{\mathbf{q}}}{\operatorname{argmin}}\, \mathcal{J}\left(\mathbf{p}, \mathbf{c}(\tilde{\mathbf{q}}^*)\right), \text{ s.t. } \mathbf{p}_{\min} \leq \mathbf{p} \leq \mathbf{p}_{\max}. \tag{13}$$

Here $\mathbf{p}_{\min}$ and $\mathbf{p}_{\max}$ are the lower and upper bounds of the parts parameters, and the objective function $\mathcal{J}$ is defined as in Equation (3). The second stage optimization has a very low number of variables compared to the first stage since the assignments are fixed and the part set is sparse. The fine-tuning explores the part space locally within a specific assignment for a local minimizer of the objective function $\mathcal{J}$. Figure 10 shows the two stage optimization process and visualizes objectives on an associated design instance. The transition between the two stages often leads to a jump in the elastic energy which is mitigated during the second stage. Figure 12 shows

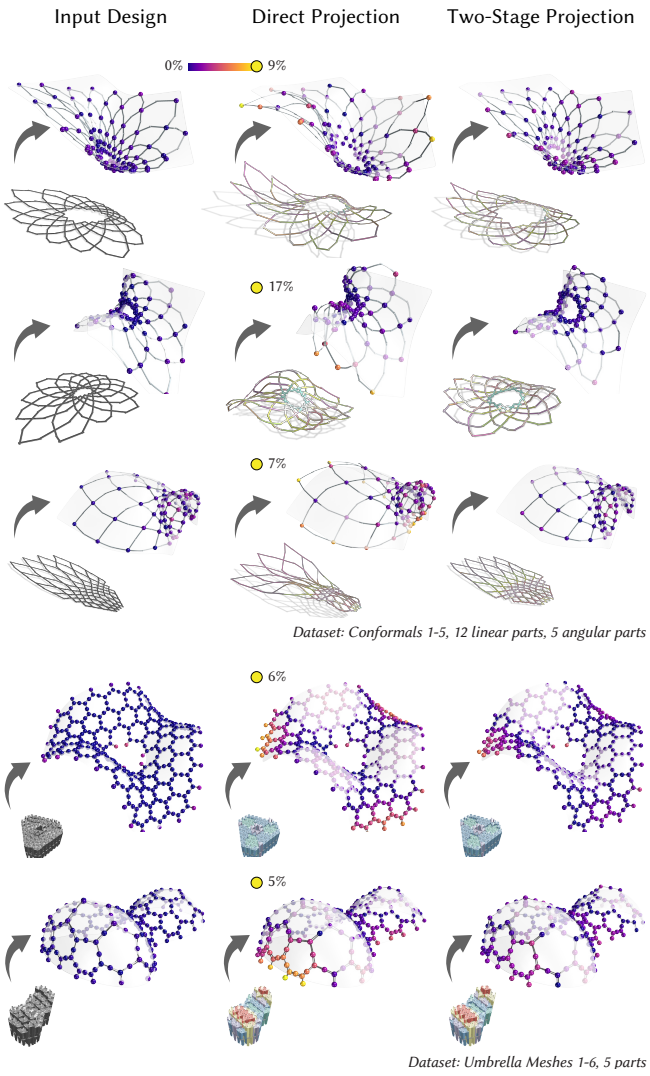

Fig. 12. We show subsets of optimized designs from two different bending-active systems after the two-stage optimization process. The left column shows the input designs, the middle column shows the designs directly projected to the part set. The right column shows the designs after the two-stage optimization process. We report the target fitting as a percentage of each model's bounding box diagonal.

the final results of the two stage optimization process for C-shells and Umbrella Meshes and compares them to the input designs as well as a direct rationalization approach.

7.3 Optimization Algorithm

We solve the optimization problems in Equation (12) and Equation (13) using a trust-region active-set method (Sequential Linear-Quadratic Programming) with a BFGS Hessian approximation [Nocedal and Wright 2006] provided by Knitro [Waltz and Nocedal 2004]. We compute the gradient of the preservation energy $\mathcal{F}$ using

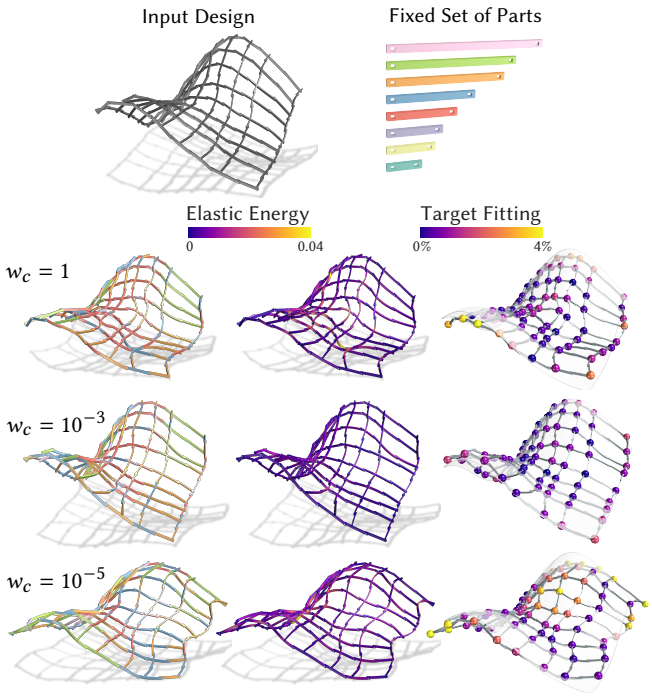

Fig. 13. A new design is projected onto an existing kit of parts. The input design has not been used during the optimization of the kit of parts. Tuning the clustering weight allows recovering a better design.

first order adjoint sensitivity analysis. More details on how differentiation with respect to the constrained simulation variables $\mathbf{x}_f^{\text{tgt}}(\mathbf{d})$ is performed can be found in the supplemental material.

We use uniform material properties for all the structures in our experiments with Young's modulus E and Poisson's ratio ν set to $(1400\text{MPa}, 0.35)$ for Umbrella Meshes, and $(2100\text{MPa}, 0.35)$ for Orthogonal Grids and C-shells. Our first stage optimization typically converges in 10 minutes to an hour on the examples we show. The second stage optimization runs faster, and typically takes no more than 15 minutes to converge in our experiments.

8 DISCUSSION

Projection onto an Existing Kit of Parts. Given an existing kit of parts $\bar{\mathbf{p}}$, our relaxation approach can project an input design onto this kit to find the best assembly that approximates the new design. Given the fixed parts, the relaxed optimization problem from Equation (4) models only the assignments $\mathbf{c}$ as dependent variables instead of both $(\mathbf{p}, \mathbf{c})$. The projection energy $\mathcal{P}$ in Equation (6) becomes $\min_{\mathbf{c}} \tilde{\mathcal{P}}(\bar{\mathbf{p}}, \mathbf{c}, \mathbf{q})$, for the choice of $\bar{\mathbf{p}}$. Figure 13 shows that a higher projection energy weight w_c enforces a tighter and quicker fit of each element to their initial assignment, preventing them from evolving during the projection operation. Lowering w_c allows smoothly transitioning from the input design to the kit of parts, leading to better assignments in practice. However, if the weight is too low, the elements are fit loosely to the parts, subsequently leading to undesired buckling once assigned to the parts.

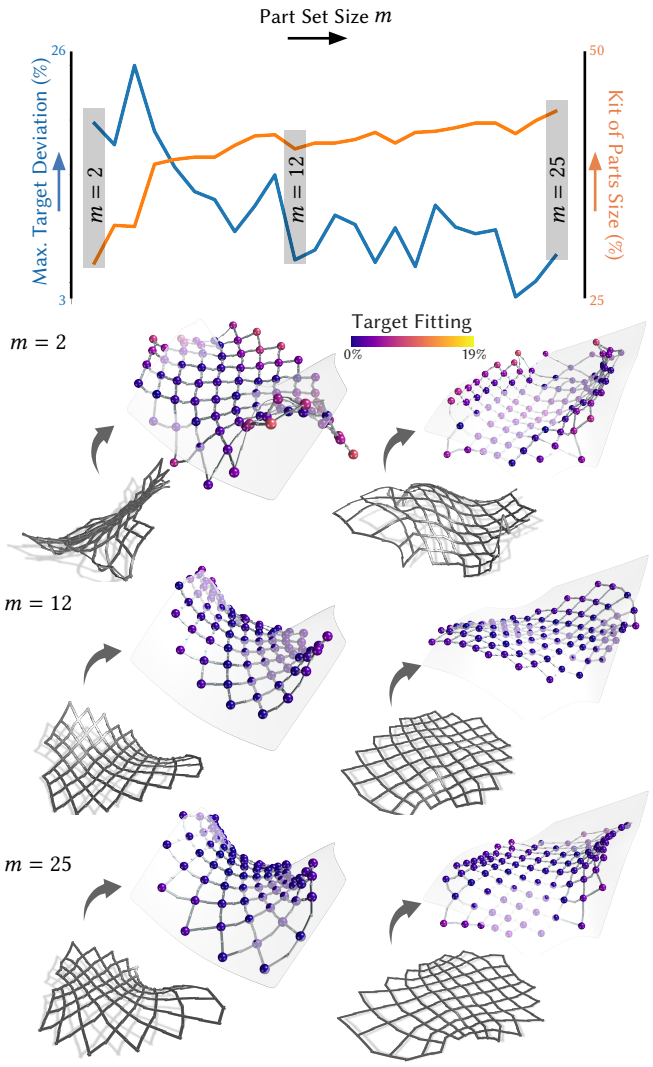

Dataset: Conformals 1-5, 2-25 linear parts, 5 angular parts

Fig. 14. Increasing the number of distinct parts m trades design fidelity for parts reuse. We jointly optimize 5 designs using the relaxation and show the resulting equilibrium states (of 2 designs) after assigning parts to elements. The kit of parts size is shown as a percentage of the total number of fabricated pieces over the total number of elements in the input designs.

Part Reuse. Consider the scenario where we fabricate only as many pieces (instances of parts) as needed such that all the designs can be realized individually using this kit of parts. When we use a small part set, the number of fabricated pieces is low, but the design fidelity can suffer due to the limited expressiveness of the parts. On the other hand, a large part set requires more pieces to be fabricated. Our framework can be used to investigate the trade-off between design fidelity and the size of the kit of parts. Figure 14 illustrates the interplay between the kit-of-parts size and the maximum deviation of the design instances from their target surfaces. In the visualized examples of rationalized designs, we observe clear improvement in the target fitting as the number of parts increase, however leading to

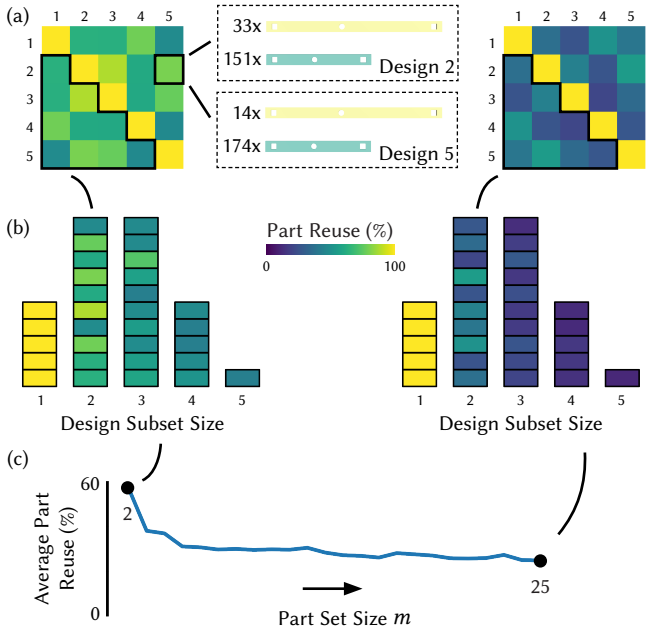

Dataset: Conformals 1-5, 2-25 linear parts, 5 angular parts

Fig. 15. (a) Pairwise Jaccard similarities between two design instances for two different part set sizes (2, 25). The inset shows the pieces used in two designs (Design 2 and Design 5, with a part set size of 2) explaining the part reuse % in the incidence matrix measuring pairwise part reuse. (b) Generalized subset-wise part reuse. Note that the pairwise similarities correspond to similarities on subsets of cardinality 2. (c) Evolution of average part reuse across all subsets with the part set size.

an increase in the total number of fabricated pieces. Notice that the gain in target fitting diminishes after a certain number of parts (12 in Figure 14), suggesting that the additional parts do not contribute significantly to the design fidelity. Thus, our framework enables discovery of the most suitable trade-off between design fidelity and fabrication complexity.

With more parts, the likelihood of reusing pieces across different designs decreases. Ideally, we would like to reuse the same pieces across different designs to maximize part reuse. For the five design instances considered in our experiments, we analyze part reuse among different subsets of designs for each part set size. For example, consider the sets of pieces $\mathcal{S}_1, \mathcal{S}_2$ used to assemble two designs respectively. Then the Jaccard similarity $|\mathcal{S}_1 \cap \mathcal{S}_2|/|\mathcal{S}_1 \cup \mathcal{S}_2|$ measures the part reuse between the two designs. Figure 15a shows the pairwise Jaccard similarities for the five design instances for two different part set sizes (2, 25). This notion can be extended to more than two designs by considering $|\bigcap_k \mathcal{S}_k|/|\bigcup_k \mathcal{S}_k|$. Visualizing part reuse among different subsets (Figure 15b) can provide insights into disconnected design subsets. A similar analysis can be done over the part subsets to discover disconnected part subsets in the kit of parts. As the number of distinct parts increases, the average part reuse diminishes, as shown in Figure 15c.

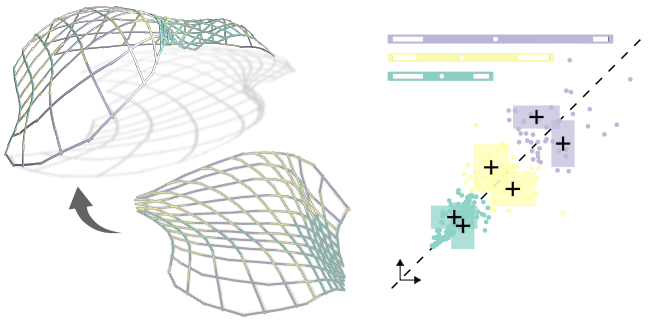

Fig. 16. Our framework can accommodate optimizing more complex part typologies. Here we extend Orthogonal Grids' and C-shells' linear parts to include slits at the ends and allow realizing several element lengths by placing the *corner* at any point along the slit.

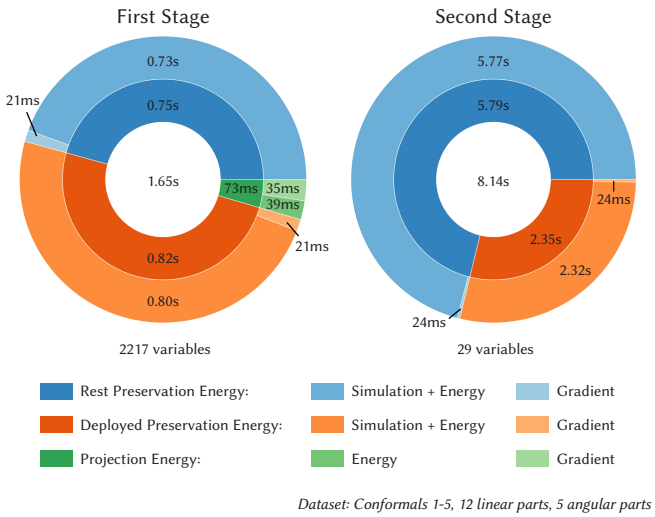

Fig. 17. Timings of our two-stage optimization, reported per each successful line search step as measured on a Linux workstation with a 64-Core AMD Ryzen Threadripper 3990X Processor and 128GB of RAM. The simulation time consists of solving the equilibrium problem possibly multiple times during the linesearch phase of the optimization. Gradient computation relies on the simulation output and is done once per step. For this experiment, the first stage took 1019 steps, and the second stage took 42 steps.

Buckling Issues During Projection. Figure 8 shows how a direct projection of elements to parts can lead to undesired buckling even for a single design. Once such a bad assignment is made, optimizing the part parameters does not recover the design fidelity as seen in Figure 11. This is because the design objective is a highly non-linear, non-convex function of the rest variables. If elements are projected to parts when the clusters are not *tight* enough, the objective can incur a large jump sometimes manifested as the observed buckling. This problem is pronounced in the case of Umbrella Meshes which have multiple stable configurations owing to a larger design space, making recovery from buckled states hard.

Our relaxation provides a continuous balance between the objectives and brings the elements $\tilde{\mathbf{q}}$ closer to the parts $\mathbf{p}$ first while maintaining the design fidelity. The auxiliary variables $\tilde{\mathbf{q}}$ are then projected to the parts $\mathbf{p}$ at the start of the second stage optimization as described in Section 7.2. Minimizing the relaxation objective $\mathcal{J}(\tilde{\mathbf{q}})$ in the first stage brings the elements $\tilde{\mathbf{q}}$ *tightly* close to the cluster center parts $\mathbf{p}$ controlled by w_c. While this is a significantly better state to project the elements to parts compared to the direct approach, it is unclear how *tight* the clustering should be. Owing to the highly nonlinear design objective, the equilibrium state can show large deviations for small changes in the element size resulting in failure cases like shown in Figure 18. In these scenarios, we increase the projection energy weight w_c before projection to explore better solutions without losing too much design fidelity. When that fails, we understand that the tight cluster of elements cannot be replaced by the cluster center part for this design, and re-initialize the clusters with a larger kit of parts.

Part Complexity. In our work, we show a kit-of-parts approach that first discretizes the input bending-active designs into atomic elements and then maps these elements to a part set that is parametrized the same way as each of the elements. We demonstrate results for three bending-active systems using this approach. However, our framework is general and can be extended to include more complex parts that are parametrized differently from the elements. For example, we can include parts that allow continuous adjustments.

Figure 16 shows an example of such more complex parts. Each straight beam has a slit window in which it can be connected to its neighboring elements. With the slits on both ends, the same part could then be used to replace multiple different elements. However, a compromise on the slit length must be found to preserve the structural integrity of the designs. Similarly, a reconfigurable umbrella part [Kusupati et al. 2023] can be used to replace multiple umbrella cells of different arm lengths that fall in the reconfigurable range. Reconfigurable elements provide additional degrees of freedom to find better solutions for the constrained problem of finding an optimal kit of parts. While complex reconfigurable parts have a greater degree of expressiveness, they also increase the fabrication complexity and can make assembly more difficult. For example, for the slitted parts shown here, parts need to be connected carefully to ensure the slit windows align correctly. In addition, the reconfigurable parts have additional components that can lead to collisions during deployment, or undesired aesthetics. We leave the thorough exploration of these reconfigurable part types for future work.

Computation Time. Figure 17 shows that most of the computation time is allocated to finding equilibria, which happens during the linesearch phase of the optimization. The gradient computation is done once per step and is relatively fast.

The optimization steps taken in the unrelaxed problem are on average more costly mainly due to a higher number of linesearch steps. The reduction from 2217 element variables to 29 part variables can explain that discrepancy. A perturbation in one of the part variables may impact more than 75 elements on average at once, in different ways depending upon their locations in their respective structures. The objective in the second stage appears more sensitive to each variable, making the optimization problem harder to solve.

The relaxed problem, on the other hand, requires fewer linesearch steps. The relaxation allows the elements to update independently and tracks a better-behaved equilibrium state.

Architectural Applications. As discussed in the introduction, bending-active structures are of particular interest in architecture. However, few designs have been realized, partly because of high cost and complexity of custom fabrication. The kit-of-parts approach that we propose can potentially alleviate these issues. In Figure 19 we show some speculative designs realized with our optimized kit of parts to illustrate the potential for applications in architecture.

9 LIMITATIONS AND FUTURE WORK

Buckling Mitigation. While the relaxation approach performs well in our experiments, we currently cannot quantify how close the solution of the relaxed version is to the optimal part set and assignment. Depending on the energy landscape of the equilibrium that is being tracked, a small perturbation in the element parameters can lead to a significant change in the objective $\mathcal{J}$. When the solution from the relaxation problem is such an equilibrium state, we observe a jump (buckling) between the two stages of the optimization, which leads to potentially irrecoverable deployed state. Figure 18 exemplifies this. Since our optimization relies on local sensitivity information we cannot easily predict when such a jump will occur.

Focused Objectives. When optimizing the part geometries, we currently do not directly control re-use efficiency i.e., the number of parts shared among different designs. If structures are to be assembled in sequence, it would be desirable if the next design could re-use as many parts from the previous design as possible to limit the total number of elements that need to be fabricated. A corresponding objective can be integrated into our optimization in future work.

While we currently use an elastic energy term in the design preservation to favor low-energy designs, we can also include focused objectives like the maximum stress in the structure. Similarly, precise load-bearing behavior can be enforced by including external loads as part of the equilibrium simulation. Incorporating these specific scenarios into our framework remains a future work.

Input Design Harmonization. Within each dataset, our input structures are designed such that initial elements belong to the same region of the element parameters space. This manual harmonization pre-processing step is necessary to ensure that the downstream optimization converges to parts shared across most designs. Automatically diagnosing the quality of the input designs and providing feedback e.g., in the form of rescaling or topology changes, on how to update the input designs best to make them more compatible with each other can be a valuable addition. This can keep users informed of the re-use efficiency during early design stages.

Fabrication. The simulation frameworks of the three bending-active systems are based on the discrete elastic rod model [Bergou et al. 2008] which has been extensively validated [Romero et al. 2021]. Umbrella Meshes and C-shells fabricate physical prototypes to validate the simulation results. Our rationalization choices to build these systems with a kit-of-parts do not alter the fabrication process and our simulation uses the same frameworks. However, it is necessary to validate the rationalized designs with physical prototypes given the sensitivity of the equilibrium states. We leave this for future work since designing easily reconfigurable systems also comes with significant engineering challenges.

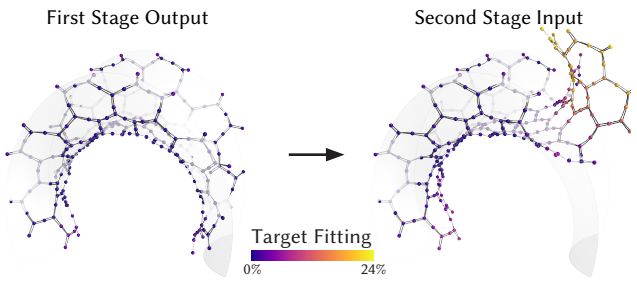

Fig. 18. A failure case of the relaxation approach in between the two stages of the optimization. Slight perturbations in the assembly rest state may result in irrecoverable buckling configurations.

10 CONCLUSION

An optimized kit of parts enables cost-effective and re-use-friendly manufacturing of complex structures. The kit-of-parts approach is particularly attractive for bending-active structures since each part can appear in different configurations i.e., deformed states, of different structures resulting in non-trivial coupling compared to rigid kit-of-parts assemblies. Furthermore, these structures sharing parts are highly sensitive to perturbations of the part geometries due to active bending. Our computational pipeline enables evaluating the trade-offs between the design preservation of input designs and part set size, by leveraging physical simulation of the bending-active equilibria to guide the optimization of the kit of parts.

ACKNOWLEDGMENTS

We thank Florin Isvoranu for his help in producing Figure 19 and for the insightful discussions about practical challenges in fabricability of a kit of parts. This research was supported by the Swiss National Science Foundation (Grant 188582).

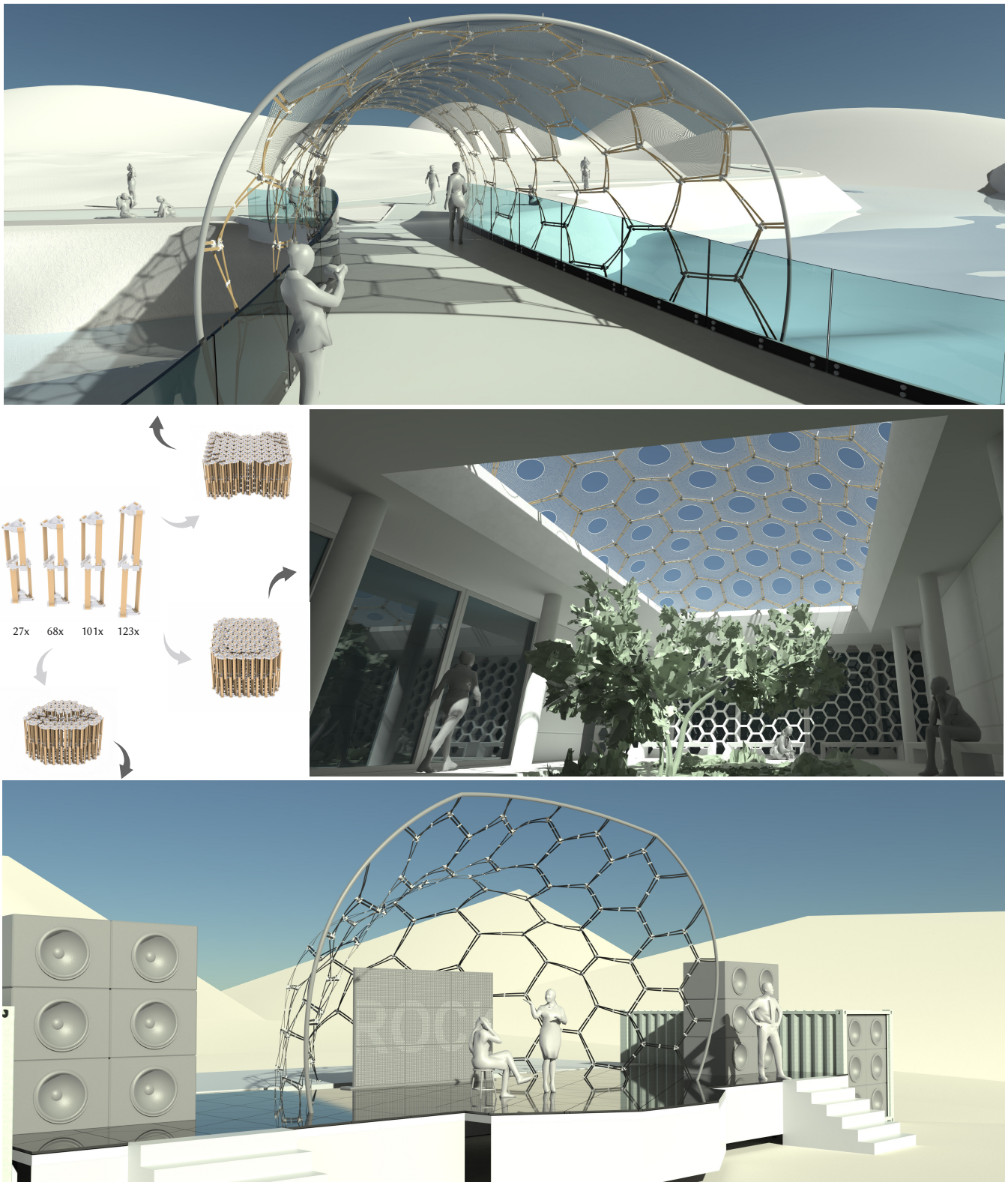

Fig. 19. Architectural applications: Speculative designs realized with an optimized kit of parts.

REFERENCES

Lara Alegria Mira, Ashley P Thrall, and Niels De Temmerman. 2016. The universal scissor component: optimization of a reconfigurable component for deployable scissor structures. *Engineering optimization* 48, 2 (2016), 317–333.

David Arthur, Sergei Vassilvitskii, et al. 2007. k-means++: The advantages of careful seeding. In *Soda*, Vol. 7. 1027–1035.

Changyeob Baek, Andrew O Sageman-Furnas, Mohammad K Jawed, and Pedro M Reis. 2018. Form finding in elastic gridshells. *Proceedings of the National Academy of Sciences* 115, 1 (2018), 75–80.

Paolo Basso, Andrea E Del Grosso, Alberto Pugnale, and Mario Sassone. 2009. Computational morphogenesis in architecture: Cost optimization of free-form grid shells. *Journal of the international association for shell and spatial structures* 50, 3 (2009), 143–150.

Quentin Becker, Seiichi Suzuki, and Mark Pauly. 2024. Interactive Design of C-shells Using Reduced Parametric Families. In *Proceedings of the IASS Annual Symposium*. International Association for Shell and Spatial Structures (IASS).

Quentin Becker, Seiichi Suzuki, Yingying Ren, Davide Pellis, Francis Julian Panetta, and Mark Pauly. 2023. C-shells: Deployable Gridshells with Curved Beams. *ACM Transactions on Graphics* 42, 6 (2023), 1–17.

Miklós Bergou, Basile Audoly, Etienne Vouga, Max Wardetzky, and Eitan Grinspun. 2010. Discrete viscous threads. *ACM Transactions on graphics (TOG)* 29, 4 (2010), 1–10.

Miklós Bergou, Max Wardetzky, Stephen Robinson, Basile Audoly, and Eitan Grinspun. 2008. Discrete elastic rods. *ACM Transactions on Graphics (TOG)* 27, 3 (2008), 1–12.

Jan Brütting, Gennaro Senatore, and Corentin Fivet. 2021. Design and fabrication of a reusable kit of parts for diverse structures. *Automation in Construction* 125 (2021), 103614.

Steinar Hillersøy Dyvik, Bendik Manum, and Anders Rønnquist. 2021. Gridshells in recent research—a systematic mapping study. *Applied Sciences* 11, 24 (2021), 11731.

Michael Eigensatz, Mario Deuss, Alexander Schiftner, Martin Kilian, Niloy J Mitra, Helmut Pottmann, and Mark Pauly. 2010. Case studies in cost-optimized paneling of architectural freeform surfaces. In *Advances in architectural geometry 2010*. Springer, 49–72.

Corentin Fivet and Jan Brütting. 2020. Nothing is lost, nothing is created, everything is reused: structural design for a circular economy. *The Structural Engineer* 98, 1 (2020), 74–81.

Chi-Wing Fu, Chi-Fu Lai, Ying He, and Daniel Cohen-Or. 2010. K-set tilable surfaces. *ACM transactions on graphics (TOG)* 29, 4 (2010), 1–6.

Grégoire Gaudreault and Andrei Nejur. 2023. Heteromorph: Temporary shelters made of reclaimed heterogeneous materials. In *Proceedings of eCAADe*. 59–68. https://doi.org/10.52842/conf.ecaade.2023.2.059

A Scott Howe, Isamu Ishii, and Tomohiro Yoshida. 1999. Kit-of-parts: A review of object-oriented construction techniques. In *ISARC'99: international symposium on automation and robotics in construction (Madrid, 22-24 September 1999)*. 165–171.

Yijiang Huang, Latifa Alkhayat, Catherine De Wolf, and Caitlin Mueller. 2021. Algorithmic circular design with reused structural elements: method and tool. In *Proceedings of the International fib Symposium on the Conceptual Design of Structures*, Vol. 55. Fédération Internationale du Béton (fib), 457–468.

Caigui Jiang, Hui Wang, Victor Ceballos Inza, Felix Dellinger, Florian Rist, Johannes Wallner, and Helmut Pottmann. 2021. Using isometries for computational design and fabrication. *ACM Transactions on Graphics (TOG)* 40, 4 (2021), 1–12.

Caigui Jiang, Jun Wang, Johannes Wallner, and Helmut Pottmann. 2014. Freeform honeycomb structures. *Computer Graphics Forum* 33, 5 (2014), 185–194.

Uday Kusupati, Florin Isvoranu, Seiichi Suzuki, and Mark Pauly. 2023. RUM: Reconfigurable Umbrella Mesh. *Advances in Architectural Geometry 2023* (2023), 474.

Riccardo La Magna. 2017. *Bending-Active Plates: Strategies for the Induction of Curvature through the Means of Elastic Bending of Plate-based Structures*. Universität Stuttgart Inst. f. Tragkonstr.

Julian Lienhard. 2014. *Bending-Active Structures: Form-finding Strategies Using Elastic Deformation in Static and Kinetic Systems and the Structural Potentials Therein*. Universität Stuttgart Inst. f. Tragkonstr.

Julian Lienhard, Holger Alpermann, Christoph Gengnagel, and Jan Knippers. 2013. Active Bending, a Review on Structures where Bending is Used as a Self-Formation Process. *International Journal of Space Structures* 28, 3-4 (2013), 187–196. https://doi.org/10.1260/0266-3511.28.3-4.187 arXiv:https://doi.org/10.1260/0266-3511.28.3-4.187

Daoming Liu, Davide Pellis, Yu-Chou Chiang, Florian Rist, Johannes Wallner, and Helmut Pottmann. 2023b. Deployable strip structures. *ACM Trans. Graph.* 42, 4, Article 103 (jul 2023), 16 pages. https://doi.org/10.1145/3592393

Yuanpeng Liu, Ting-Uei Lee, Antiopi Koronaki, Nico Pietroni, and Yi Min Xie. 2023a. Reducing the number of different nodes in space frame structures through clustering and optimization. *Engineering Structures* 284 (2023), 116016.

Yizhe Liu, Fei Pan, Bin Ding, Yilong Zhu, Kuijian Yang, and Yuli Chen. 2022. Multistable shape-reconfigurable metawire in 3D space. *Extreme Mechanics Letters* 50 (2022), 101535.

Zhong-Yuan Liu, Zhan Zhang, Di Zhang, Chunyang Ye, Ligang Liu, and Xiao-Ming Fu. 2021. Modeling and fabrication with specified discrete equivalence classes. *ACM Trans. Graph.* 40, 4, Article 41 (jul 2021), 12 pages. https://doi.org/10.1145/3450626.3459843

Hongjia Lu and Yi Min Xie. 2023. Reducing the number of different members in truss layout optimization. *Structural and Multidisciplinary Optimization* 66, 3 (2023), 52.

Sheng-Jie Luo, Yonghao Yue, Chun-Kai Huang, Yu-Huan Chung, Sei Imai, Tomoyuki Nishita, and Bing-Yu Chen. 2015. Legolization: Optimizing lego designs. *ACM Transactions on Graphics (TOG)* 34, 6 (2015), 1–12.

James MacQueen et al. 1967. Some methods for classification and analysis of multivariate observations. In *Proceedings of the fifth Berkeley symposium on mathematical statistics and probability*, Vol. 1. Oakland, CA, USA, 281–297.

Iason Manolas, Francesco Laccone, Gianmarco Cherchi, Luigi Malomo, Paolo Cignoni, et al. 2022. A Computational Tool for the Analysis of 3D Bending-active Structures Based on the Dynamic Relaxation Method.. In *STAG*. 1–9.

Romain Mesnil, Takara Muto, Krittika Walia, Cyril Douthe, and Olivier Baverel. 2023. *Design and Fabrication of a Pseudo-Geodesic Gridshell*. De Gruyter, Berlin, Boston, 83–96. https://doi.org/doi:10.1515/9783111162683-007

Jorge Nocedal and Stephen Wright. 2006. *Numerical optimization*. Springer Science & Business Media.

Julian Panetta, Mina Konaković-Luković, Florin Isvoranu, Etienne Bouleau, and Mark Pauly. 2019. X-shells: A new class of deployable beam structures. *ACM Transactions on Graphics (TOG)* 38, 4 (2019), 1–15.

Stefan Pillwein and Przemyslaw Musialski. 2021. Generalized deployable elastic geodesic grids. *ACM Transactions on Graphics (TOG)* 40, 6 (2021), 1–15.

Yingying Ren, Uday Kusupati, Julian Panetta, Florin Isvoranu, Davide Pellis, Tian Chen, and Mark Pauly. 2022. Umbrella meshes: elastic mechanisms for freeform shape deployment. *ACM Transactions on Graphics* 41, ARTICLE (2022), 1–15.

Victor Romero, Mickaël Ly, Abdullah Haroon Rasheed, Raphaël Charrondière, Arnaud Lazarus, Sébastien Neukirch, and Florence Bertails-Descoubes. 2021. Physical validation of simulators in Computer Graphics: A new framework dedicated to slender elastic structures and frictional contact. *ACM Transactions on Graphics (TOG)* 40, 4 (2021), 1–19.

Eike Schling. 2018. *Repetitive Structures*. Ph. D. Dissertation. Technische Universität München. https://mediatum.ub.tum.de/1449869

Eike Schling and Rainer Barthel. 2020. Repetitive structures. In *Impact: Design With All Senses: Proceedings of the Design Modelling Symposium, Berlin 2019*. Springer, 360–375.

Eike Schling, Martin Kilian, Hui Wang, Jonas Schikore, and Helmut Pottmann. 2018. Design and construction of curved support structures with repetitive parameters. In *Advances in Architectural Geometry*. https://api.semanticscholar.org/CorpusID:54173491

Eike Schling, Hui Wang, Sebastian Hoyer, and Helmut Pottmann. 2022. Designing asymptotic geodesic hybrid gridshells. *Computer-Aided Design* 152 (2022), 103378.

Mayank Singh and Scott Schaefer. 2010. Triangle surfaces with discrete equivalence classes. *ACM Transactions on Graphics (TOG)* 29, 4 (2010), 1–7.

Caroline St-Hilaire and Andrei Nejur. 2022. WoodN - In search of a constructive system for a sustainable temporary architecture. In *Proceedings of eCAADe*. 185–194. https://doi.org/10.52842/conf.ecaade.2022.1.185

Xavier Tellier. 2022. Bundling elastic gridshells with alignable nets. Part I: Analytical approach. *Automation in Construction* 141 (2022), 104291.

Romain Pierre Testuz, Yuliy Schwartzburg, and Mark Pauly. 2013. Automatic generation of constructable brick sculptures. *Eurographics 2013-Short Papers* (2013), 81–84.

Richard A Waltz and Jorge Nocedal. 2004. KNITRO 2.0 User's Manual. *Ziena Optimization, Inc.[en ligne] disponible sur http://www. ziena. com (September, 2010)* 7 (2004), 33–34.

Xudong Yang, Yuan Zhou, Huichan Zhao, Weicheng Huang, Yifan Wang, K. Jimmy Hsia, and Mingchao Liu. 2023. Morphing matter: from mechanical principles to robotic applications. *Soft Science* 3, 4 (2023). https://doi.org/10.20517/ss.2023.42

Yinan Zhang and Devin Balkcom. 2016. Interlocking structure assembly with voxels. In *2016 IEEE/RSJ International Conference on Intelligent Robots and Systems (IROS)*. IEEE, 2173–2180.

Tianyu Zhu, Zeng-Hao Xu, Ligang Liu, and Xiao-Ming Fu. 2023. Modeling with discrete equivalence classes of planar quads. *Computers & Graphics* 115 (2023), 404–411.

Henrik Zimmer, Marcel Campen, David Bommes, and Leif Kobbelt. 2012. Rationalization of triangle-based point-folding structures. *Computer Graphics Forum* 31, 2pt3 (2012), 611–620.

Henrik Zimmer, Florent Lafarge, Pierre Alliez, and Leif Kobbelt. 2014. Zometool shape approximation. *Graphical Models* 76, 5 (2014), 390–401.